Published in final edited form as:
J Immunol. 2013 February 1; 190(3): 1285–1296. doi:10.4049/jimmunol.1202208.

TLR4 Activation Under Lipotoxic Conditions Leads to Synergistic Macrophage Cell Death Through a TRIF-Dependent Pathway[1]

Joel D. Schilling[*,†,‡], **Heather M. Machkovech**[*,†], **Li He**[*,†], **Abhinav Diwan**[†], and **Jean E. Schaffer**[*,†,2]

[*]Diabetic Cardiovascular Disease Center, Washington University School of Medicine, St. Louis, Missouri

[†]Department of Medicine, Washington University School of Medicine, St. Louis, Missouri

[‡]Department of Pathology and Immunology, Washington University School of Medicine, St. Louis, Missouri

Abstract

Macrophage dysfunction in obesity and diabetes may predispose to the development of diabetic complications such as infection and impaired healing after tissue damage. Saturated fatty acids, such as palmitate, are present at elevated concentrations in the plasma of patients with metabolic disease and may contribute to the pathogenesis of diabetes and its sequelae. To examine the effect of lipid excess on macrophage inflammatory function, we determined the influence of palmitate on LPS-mediated responses in peritoneal macrophages. Palmitate and LPS led to a profound synergistic cell death response in both primary and RAW 264.7 macrophages. The cell death had features of apoptosis and necrosis and was not dependent on ER stress, ceramide generation, or reactive oxygen species production. Instead, we uncovered a macrophage death pathway that required TLR4 signaling via TRIF, but was independent of NF-κB, MAP kinases, and IRF3. A significant decrease in macrophage lysosomal content was observed early in the death pathway, with evidence of lysosomal membrane damage occurring later in the death response. Over-expression of the transcription factor TFEB, which induces a lysosomal biogenic program, rescued the lysosomal phenotype and improved viability in palmitate and LPS treated cells. Our findings provide new evidence for crosstalk between lipid metabolism and the innate immune response that converges on the lysosome.

Introduction

Obesity and diabetes and their related complications are associated with significant morbidity, mortality, and increased health care costs. Impaired responses to tissue damage are a common feature of many diabetic complications, leading to adverse outcomes from infectious and non-infectious injury, including myocardial infarction and surgery (1–4). Despite extensive epidemiologic data, the mechanisms underlying the inflammatory and wound repair phenotype in diabetics remains poorly understood. Given the central role of macrophages in the regulation of inflammation and tissue healing, dysfunction of these cells

[1]This work was supported by grants from the NIH (R01 DK064989 and AMDCC U24 DK076169 to JES; K08HL098373 to JDS; and P60 DK020579); the Burroughs Wellcome Foundation (1005935 to JES) and the Diabetes Action Foundation (to JDS).

[2]Address correspondence to: Jean E. Schaffer, M.D., Diabetic Cardiovascular Disease Center, Washington University School of Medicine, St. Louis, MO 63110, jschaff@wustl.edu.

in diabetes has been proposed to contribute to the pathogenesis of diabetic complications (5–8).

Macrophage activation in response to pathogens and/or tissue damage occurs in part through toll-like receptors (TLRs) (9, 10). In particular, TLR4 is a sensor that responds to both pathogen-associated molecular patterns, such as LPS, and tissue damage related signals, such as high-mobility group box 1 protein (HMBG1) (11, 12). Consistent with this, TLR4 knockout (KO) mice have reduced inflammation in response to gram-negative bacterial infection as well as to sterile tissue injury such as myocardial infarction (13, 14). TLR4 is a cell surface receptor that activates two distinct intracellular signaling pathways via the adaptor molecules MyD88 and TRIF (15). MyD88-dependent signaling triggers the classical inflammatory cascade resulting in NF-κB and MAP kinase activation. On the other hand, TRIF associates with TLR4 after ligand-induced internalization and leads to activation of IRF3 and interferon-β production. TRIF-dependent signaling can also mediate delayed NF-κB and MAP kinase activation and has been implicated in some cell death signaling pathways (16).

Emerging evidence shows that the metabolic perturbations in obesity and diabetes influence macrophage biology. For example, lipid excess promotes macrophage recruitment to adipose tissue and can shift macrophage polarization towards a more inflammatory phenotype (17, 18). Long chain saturated fatty acids such as palmitate and stearate are increased in the plasma and tissues of obese and diabetic individuals and are thought to contribute to organ dysfunction underlying diabetes progression and the pathogenesis of complications (19, 20). In vitro exposure of endothelial cells, fibroblasts, pancreatic β-cells, hepatocytes, and myoblasts to palmitate triggers endoplasmic reticulum (ER) stress, ceramide production, and oxidative stress which can lead to lipotoxic cell death (21). The effects of palmitate on primary macrophages are less well understood, and it remains controversial whether long-chain saturated fatty acids, such as palmitate, can directly activate TLR4 on these cells (22, 23).

Premature or excessive macrophage cell death has the potential to impair inflammatory and tissue repair pathways. Therefore, we sought to evaluate how the crosstalk between palmitate and TLR4 signaling impacts macrophage survival. Herein we demonstrate that stimulation of primary macrophages with LPS under lipotoxic conditions produces a profound synergistic cell death phenotype that is dependent on TLR4. Our study uncovers a novel TRIF-dependent cell death pathway that is associated with lysosomal dysfunction and illustrate a unique mechanism by which excess lipids can promote macrophage dysfunction.

Materials and Methods

Reagents

SB203580, PD98059, SB600125, BAY 11-7085, CA-074 ME, necrostatin 1, phenybutryic acid (PBA) and staurosporine (STS) were from EMD-Millipore. ZVAD and Mito-TEMPO were from Enzo Life Sciences. Fumonisin B was from Cayman Chemicals. Ultrapure E. coli LPS was from Invivogen. Recombinant mouse TNFα was from R & D Systems. The α-cathepsin D antibody was from Abcam and the α-LAMP1 antibody was from Santa Cruz. The BHA, α-actin, α-tubulin, and the α-flag M2 antibodies were from Sigma. Thioglycollate was from Difco. Fatty acids were from Nu-Chek Prep. Ultrapure-bovine serum albumin (BSA) was from Seracare and was tested for TLR ligand contamination prior to use. AnnexinV-GFP was from BioVision. Lysotracker red, tetramethylrhodamine(TMR)-dextran (10,000 MW), and Hoechst nuclear dye were from Invitrogen; acridine orange was from Sigma. The protease inhibitor (25X Protease Complete tablets) was from Roche.

Cell Culture

Peritoneal macrophages were isolated from C57BL/6, or the indicated knockout mice 4 days after intraperitoneal injection of thioglycollate and plated at a density of 5×10^5 cells/ml in DMEM containing 10% inactivated fetal serum (IFS), 50 U/ml penicillin G sodium, and 50U/ml streptomycin sulfate (pen-strep). Stimulations were performed on the day after harvest. For flow cytometry experiments, peritoneal cells were cultured on low adherence plates (Greiner Bio-One) to facilitate cell harvest. Although some studies have reported up to 10–15% contamination of thioglycollate-elicted cells with non-macrophage cells types such as eosinophils (24), we routinely found that only 2–4% of the adherent cells were Siglec F^+, $F4/80^+$. RAW 264.7 cells (ATCC) were cultured in DMEM containing 10% IFS and pen-strep. Stably transfected HEK293 containing CD14/MD2/TLR4 or control vector were obtained from Invivogen and cultured according to the manufacturers recommendations. Growth medium supplemented was with palmitate or oleate complexed to BSA at a 2:1 molar ratio as described previously (25) and BSA-supplemented media was used as control. For cell stimulations, PBS or LPS (50 ng/ml) were added to BSA or palmitate media.

Mice

Wild type (WT) and TLR4 knockout (KO) C57BL/6 mice were obtained from Oriental Bioscience. NOX2 KO mice were from Jackson Laboratories. TRIF KO, MYD88 KO, TRIF/MYD88 DBL KO C57BL/6 mice were from Marco Colonna (Washington University); IRF3 KO mice were from Michael Diamond (Washington University); IKKβ floxed mice crossed with Lys-M Cre were from Michael Karin (UCSD). Mice were maintained in a pathogen free facility on a standard chow diet ad libitum (6 % fat). All animal experiments were conducted in strict accordance with NIH guidelines for humane treatment of animals and were reviewed by the Animal Studies Committee of Washington University School of Medicine.

Assessment of Cell Death

Annexin-PI staining—Cells were stimulated as indicated, recovered by trypsinization, and stained with AnnexinV-GFP (ANX) and propidium iodide (PI) according to manufacturer's instructions (BioVision). Samples were analyzed for green (FL1) and red (FL2) fluorescence on a Becton Dickinson FACS Scan flow cytometer with analysis of 10^4 cells/sample. Where indicated, ANX^+PI^- (apoptotic) and ANX^+PI^+ (necrotic) cells are both reported as dead cells. Data analysis was performed using Flow Jo software (Tree Star, Inc).

LDH release assay—After stimulation of 2.5×10^5 cells, supernatants were collected at the indicated time points and LDH was quantified the CytoTox 96 Non-Radioactive Cytotoxicity Assay (Promega) per the manufacturers instructions using a Tecan Infinite M200 plate reader. Total LDH content was determined using the lysis buffer provided by the manufacturer according to their protocol.

SubG1 DNA Content—SubG1 DNA content in macrophages was determined by PI staining and flow cytometry as described previously (26).

Mitochondrial Membrane Permeability (MMP)—MMP was assessed in stimulated macrophages using a Mito-ID kit (Enzo) as per the manufacturer's instructions with analysis using a Tecan Infinite M200 plate reader.

RNA isolation and Quantitative RT-PCR

Total cellular RNA was isolated using Qiagen RNeasy columns and reverse transcribed using a high capacity cDNA reverse transcription kit (Applied Biosystems). Real-time qRT-PCR was performed using SYBR green reagent (Applied Biosystems) on an ABI 7500 fast thermocycler. Relative gene expression was determined using the delta-delta CT method normalized to 36B4 expression. Mouse primers sequences were as follows (all 5′-3′): *36B4* (forward- ATC CCT GAC GCA CCG CCG TGA, reverse-TGC ATC TGC TTG GAG CCC ACG TT); *TNFα* (forward-CAT CTT CTC AAA ATT CGA GTG ACA A, reverse-TGG GAG TAG ACA CAA GGT ACA ACC C); *IFNβ* forward – GAC GGA GAA GAT GCA GAA GAG TT, reverse- AGT TCA TCC AGG AGA CGT ACA AC); *GRP78* (forward-GCC TCA TCG GAC GCA CTT, reverse-AAC CAC CTT GAA TGG CAA GAA); *CHOP* (forward-CAG ATT CCA GTC AGA GTT CTA TGG, reverse-GAC CAC TCT GTT TCC GTT TCC T).

Lysosome imaging

After the indicated stimulations, cells were stained with 500 nM lysotracker red or 1 μg/ml acridine orange in tissue culture media for 15 minutes at 37°C. For fluorescent dextran experiments, macrophages were incubated with 500 μg/ml tetramethylrhodamine (TMR)-dextran for 2 h in regular media followed by cell stimulations for 16 h. After staining, cells were washed three times with PBS, harvested as described above, and analyzed by flow cytometry. Alternatively, macrophages were cultured on glass coverslips stained with lysotracker red, fixed with 4% paraformaldehyde, stained with Hoechst nuclear dye, and mounted on glass slides for imaging. Immunofluorescence images were obtained on a Leica wide field fluorescence microscope.

Western blotting

For total cellular proteins, cells were lysed in 150 mM NaCl, 10 mM Tris (pH 8), triton X-100 1% and 1X Protease Complete. Western blotting for FLAG-TFEB, LAMP1, and actin was performed using 25 μg of total cellular protein. For cytoplasmic cathepsin D analysis following stimulation with BSA-PBS or palmitate-LPS, cytosolic proteins were recovered by extraction with digitonin buffer (150 mM NaCl, 50 mM HEPES pH 8, 50 μg/ml digitonin, 1X Complete Protease inhibitors) and concentrated using 10K Amicon Ultra centrifugal filter units (Millipore). Western blot for cathepsin D using 25 μg of cytoplamic protein was analyzed by SDS-PAGE and western blotting. Tubulin was used as a loading control.

TFEB transfection

A mammalian expression vector for exogenous expression of N-terminal FLAG tagged mouse TFEB and bi-cistronic expression of GFP was created by cloning the requisite coding sequences into the BamH1 and Xho1 sites of the backbone pAAV-CMV-IRES-hrGFP. HEK293-TLR4/CD14/MD2 cells were transfected using lipofectamine 2000 (Invitrogen). After 24 h, transfected cells were stimulated with BSA-PBS or palmitate-LPS for an additional 48 h. Samples were prepared as above for PI and lysotracker red staining and flow cytometry analysis. Transfection was assessed by GFP fluorescence and cell death was by PI staining.

Palmitate uptake and oxidation assays

Palmitate uptake assay—The palmitate uptake assay was performed as described previously (27).

Palmitate oxidation assay—Palmitate oxidation was determined as previously described (28).

C16 Ceramide Quantification

Macrophages were removed from the dish by scraping in PBS and homogenized by passing through 26 G needle 15 times. The lipids were extracted by incubating 50 μl of cell lysate with 450 μl of methanol with the addition of 50 ng C17 ceramide as a recovery standard. LC-MS/MS analysis was performed as described (29) on an API4000 LC-MS/MS. Values were normalized to DNA concentration in the lysate as determined using a Nanodrop spectrophotometer.

TNFα ELISA

Supernatants were harvested from macrophages 6 h after the indicated stimulations. TNFα was quantified using a DuoSet ELISA kit (R&D systems) according to the manufacturers instructions.

Reactive Oxygen Species (ROS) quantification

Stimulated macrophages were washed and incubated with 3 μM 5-(and-6)-chloromethyl-2′, 7′-dichlorodihydrofluorescein diacetate, acetyl ester (DCF, Invitrogen) in PBS or 5 μM MitoSOX (Invitrogen) in tissue culture media for 15 min at 37°C. Cells were removed from plates and analyzed by flow cytometry using the FL1 (DCF) or FL2 (MitoSOX) channel (10^4/cells collected per sample).

Statistics

Statistical analysis was performed using GraphPad Prism software. All results are expressed as means +/− SE. Groups were compared by paired Student's t-test or 2-way ANOVA as appropriate. A value of $p \leq 0.05$ was considered significant.

Results

LPS and palmitate trigger synergistic cell death in macrophages

To investigate the effects of dietary lipids on macrophage inflammatory responses we cultured primary peritoneal macrophages with pathophysiological concentrations of palmitate conjugated to BSA (or BSA alone as control), in combination with 50 ng/ml LPS stimulation, or PBS as control (30, 31). Analysis of both primary macrophages and the RAW 264.7 macrophage cell line by combined annexin V (ANX)-propidium iodide (PI) staining and flow cytometry at 24 h showed a significant reduction in viability with the combination of LPS and palmitate (Fig. 1A and B). In contrast, at these concentrations, LPS alone or palmitate alone produced no or minimal cell death, respectively. We also observed synergy between LPS and palmitate using an LDH release assay as an alternate measure of cell death. Treatment with palmitate and LPS led to increases in extracellular LDH, quantified as percent maximal cellular LDH or simply as quantity of LDH in media (A_{492}), since total cellular LDH levels remained constant (Fig. 1C). Synergistic cell death was dependent on the dose of palmitate and was apparent at palmitate concentrations as low as 100 μM (Fig. 1D, *left panel*), however, comparable concentrations of the unsaturated fatty acid oleate did not induce cell death when combined with LPS (Fig. 1D, *right panel*). Since lipotoxic responses can be enhanced in the presence of high glucose (32), we compared cell death in macrophages stimulated in the presence of high (4.5 g/L) or low (1 g/L) concentrations of glucose. There was no difference in macrophage cell death with palmitate-LPS treatment at these different glucose concentrations, indicating that the phenotype was

largely driven by lipid overload (Fig. 1E). Moreover, LPS did not significantly affect palmitate uptake or oxidation in the time frame of this assay (Fig. 1F).

Synergistic cell death does not require ER stress, ceramide generation, or oxidative stress

To further characterize the macrophage cell death induced by the combination of palmitate and LPS, we performed ANX-PI staining at several time points after treatment. In this analysis, cells that stain with ANX only (ANX^+PI^-) are considered to be apoptotic, whereas cells positive for both ANX and PI (ANX^+PI^+) are necrotic. A modest increase in necrotic cells was observed early, by 8 h after stimulation, and both apoptotic and necrotic cells gradually increased over time (Fig. 2A). By 24 h, cells were equally distributed between apoptotic and necrotic phenotypes. At no timepoint was there a predominance of apoptotic cells, suggesting that post-apoptotic necrosis does not account for the appearance of the double positive population. In contrast, macrophages treated with the apoptosis inducer staurosporine (STS) were predominantly ANX single positive (Fig. 2A, *far right panel*). A similar profile for apoptotic vs. necrotic death after palmitate-LPS stimulation was observed RAW 264.7 cells as well (Fig. 2B). Consistent with our observation that palmitate-LPS treatment led to apoptosis as well as necrosis, palmitate-LPS treated cells had an increase in Sub-G1 DNA, an indicator of DNA cleavage that occurs during apoptosis (Fig. 2C).

RIP1 kinase can activated by inflammatory signals and triggers a programmed form of necrosis known as necroptosis. To determine the role of this kinase in palm-LPS induced cell death we incubated macrophages with the RIP1 kinase inhibitor necrostatin 1 (nec1). Nec1 was able to block necroptotic cell death induced by TNF-ZVAD, but did not affect cell death after palmitate-LPS treatment (Fig. 2D). Caspases are cysteine proteases that are known to function as key executors of apoptotic cell death. To evaluate their role in palmitate-LPS induced death we pre-treated macrophages with the pan-caspase inhibitor ZVAD. However, this combination led to profound necrotic cell death of macrophages (Fig. 2E). Prior studies have shown that treatment with ZVAD in combination with LPS triggers necroptosis, a response dependent on RIP1 kinase and inhibited by nec1 (28, 29). When we treated macrophages with palmitate-LPS in the presence of both ZVAD and nec1, we observed only a modest (~25%) decrease in overall death compared to palmitate-LPS alone, and this reflected a primarily a decrease in the ANX single positive/apoptotic population (Fig. 2E). Consistent with the LDH release assay, Nec1 treatment alone did not reduce palmitate-LPS induced cell death of macrophages (Fig. 2E). Together, our findings suggest a model in which synergistic cell death upon treatment with palmitate and LPS involves both caspase-dependent and -independent cell death mechanisms.

Previous reports in a variety of cell types have implicated ER stress, ceramide production, and oxidative stress in the cell death induced by palmitate (33–35). This raised the possibility that LPS may amplify lipotoxic cell death by augmenting these cellular stress responses. ER stress, as measured by CHOP and GRP78 mRNA induction, was significantly upregulated in palmitate-LPS treated cells (Fig. 3A). However, treatment with the ER stress reliever phenylbutyric acid (36) failed to protect macrophages from cell death despite significantly reducing the expression of ER stress markers (Fig. 3A). C16 ceramide levels were also markedly elevated in palmitate-LPS stimulated cells, but treatment with the ceramide synthase inhibitor fumonisin B at a concentration that reduced C16 ceramide levels by 80% failed to protect macrophages from cell death (Fig. 3B). Unexpectedly, we did not observe an increase in reactive oxygen species in pMACs following palmitate-LPS treatment using DCF or MitoSOX staining (Fig. 3C). Furthermore, treatment of pMACs with the antioxidants, butylated hydroxyanisole (BHA) and mito-TEMPO (MT), did not reduce palmitate-LPS-induced cell death (Fib. 3D, *left panel*), and macrophages from mice deficient in the NADPH oxidase subunit NOX2 were not protected from palmitate-LPS induced cell death (Fig. 3D, right panel). Interestingly, RAW 264.7 macrophages did have

detectable ROS after palmitate-LPS treatment by DCF flow cytometry (Fig. 3E). However, while apocynin completely inhibited this ROS production, it failed to significantly reduce cell death in these cells (Fig. 3E). To determine whether pMACs failed to generate a ROS response as a consequence of maximal activation during isolation, we also assessed TNFα release in response to LPS. Using this measure of activation, pMACs were more quiescent than the RAW cells at baseline, and generated a robust TNFα response to LPS stimulation (Fig. 3F), a finding that argues against maximal pre-activation. Together, these findings suggest that ER stress, ceramide production, or oxidative stress alone is not sufficient to explain macrophage death produced by palmitate and LPS.

Synergistic cell death requires TLR4, but is independent of NF-κB and MAP kinase activation

Canonical LPS signaling occurs through the TLR4 receptor. To establish the role of TLR4 signaling in the synergistic cell death response, we utilized pMACs from wild type and TLR4 knockout (KO) mice. Only TLR4-expressing cells underwent cell death upon co-treatment with palmitate and LPS (Fig. 4A). Of note, the modest toxicity seen with palmitate treatment alone was not reduced in the absence of TLR4, indicating that the lipid-only response in these cells is TLR4-independent. To further assess the contributions of TLR4, we examined cell death in the TLR4 deficient cell line HEK 293 at baseline and following stable overexpression of the LPS receptor complex (TLR4/MD2/CD14). These cells serve as a model system for TLR signaling that reconstitutes downstream activation of NF-κB and IRF3 and provide a highly transfectable cell background in which to study TLR-mediated signaling pathways (37–40). Cell death was modestly increased by palmitate alone in parental and TLR4/MD2/CD14-expressing cells; however, only TLR4/MD2/CD14-expressing cells showed an augmentation of death with LPS (Fig. 4B), similar to findings in pMACs and RAW 264.7 cells.

Since TLR4 signaling triggers activation of NF-κB and the MAP kinases p38, JNK, and ERK, we probed these signaling pathways using well-established inhibitors of these molecules. To reduce NF-κB activation we used the I-κ kinase inhibitor BAY 11-7085 and macrophages from mice deficient in IKK-β. Although BAY11-7085 reduced TNFα secretion ~75%, there was no significant effect on the cell death response to palmitate-LPS (Fig 4C). Consistent with this result, IKK-β knockout macrophages had a similar cell death phenotype, compared to WT cells, after palmitate-LPS treatment (Fig. 4D). MAP kinase inhibitors (SB203580 for p38, PD98059 for ERK, and SP600125 for JNK) also failed to reduce synergistic cell death at concentrations that effectively modulated TNF release (Fig. 4E). Together this data indicates that TLR4 is required for palmitate-LPS cell death, but that this pathway does not require its canonical inflammatory signaling pathways.

TRIF is required for Palmitate-LPS synergistic cell death

Amongst the earliest events following TLR4 ligation is its association with the adaptor proteins MyD88 and TRIF, each of which initiates distinct signaling pathways. To address the downstream pathway relevant to palmitate-LPS mediated synergistic death, macrophages were isolated from MyD88 KO, TRIF KO, and MyD88-TRIF KO (DBL KO) mice. After stimulation with vehicle or palmitate in the presence of PBS or LPS, cell death was determined by LDH release (Fig. 5A). Macrophages from WT and MyD88 KO cells demonstrated similar cell death phenotypes; however, TRIF KO macrophages were significantly protected from synergistic cell death. Macrophages from mice lacking both MyD88 and TRIF were completely protected from the effect of LPS on lipotoxicity. We confirmed the importance of TRIF-mediated signaling in the cell death phenotype by ANX-PI staining of WT vs. TRIF KO macrophages challenged with LPS and palmitate (Fig. 5B). Consistent with our data from TLR4KO mice, TRIF deficient macrophages were protected

from synergistic cell death but not the modest baseline toxicity of palmitate (Fig. 5B). Thus, TLR4-TRIF signaling is required for the observed synergistic macrophage cell death phenotype upon challenge with palmitate and LPS.

The TRIF signaling cascade leads to the activation of the transcription factor IRF3 and the induction of IFNβ. To determine whether IRF3 activation is required downstream of TRIF in this cell death pathway, macrophages from IRF3 KO mice were stimulated with palmitate-LPS. Surprisingly, IRF3 KO macrophages were not protected from palmitate-LPS mediated cell death (Fig. 5C). As expected, IFNβ mRNA was not induced by LPS treatment of IRF3 KO cells (Fig. 5D). Thus, TLR4-mediated TRIF signaling modulates synergistic cell death through an IRF3-independent mechanism.

Cell death induced by palmitate and TLR4 activation is associated with lysosomal depletion and destablization

Palmitate treatment leads to membrane remodeling, a process linked to dysfunction of intracellular organelles (41, 42). Given evidence that lysosome dysfunction can induce cell death through caspase-dependent and -independent mechanisms (43), we evaluated the impact of LPS and palmitate on macrophage lysosomes. Lysotracker red fluorescence in macrophages treated with either LPS or palmitate was slightly reduced compared to control treated cells when analyzed by flow cytometry. However, combined palmitate-LPS treatment of macrophages caused a marked reduction in lysotracker red signal (Fig. 6A, B, and C). Function of the lysosomal compartment was also assessed using tetramethylrhodamine (TMR)-dextran to label the lysosomes and late endosomes. Palmitate and palmitate-LPS treatment produced a significant decrease in the TMR-dextran signal, suggesting that the normal lysosomal compartment is impaired or depleted (Fig 6D). The downshift in lysosomal fluorescence identified with lysotracker staining was evident as early as 8 h after stimulation and preceded the loss of mitochondrial membrane potential and increase in ANX staining (Fig. 6E).

Diminished staining with lysomotrophic dyes can result from lysosome depletion and/or lysosomal membrane permeablization (LMP), both of which have been associated with lysosomal-mediated cell death (44, 45). We used two complementary approaches to assess LMP in palmitate-LPS-stimulated macrophages. Acridine orange is a lysomotropic dye that fluoresces red/orange (FL3 channel) at high concentrations, such as in the lysosome, and green (FL1 channel) when present at low concentrations, such as in the cytosol. LMP causes a reduction in red fluorescence with a concomitant increase in green fluorescence (46). In macrophages treated with palmitate-LPS, we observed a decrease in red fluorescence (FL3) with a concomitant increase in green fluorescence (FL1), which is consistent with palmitate-LPS-induced LMP (Fig. 6F). Furthermore, during LMP, release of cathepsins into the cytosol is associated with cell death (47). In macrophages treated with palmitate-LPS, cathepsin D protein increased in the cytosol and this response was blunted in TRIF deficient macrophages (Fig. 6G). To address the contribution of cathepsin release to cell death from palmitate-LPS challenge, we pre-treated stimulated macrophages with the cathepsin B inhibitor, CAO-74. Inhibition of cathepsin B partially protected cells from palmitate-LPS induced cell death (Fig. 6H). We also assessed the lysosomal phenotype in TRIF KO macrophages after palmitate-LPS treatment. Whereas the decrease in lysotracker red signal in WT macrophages was exacerbated with the combined LPS and palmitate stimulus over either stimulus alone (Figs. 6A and 6I, *black vs. blue or green lines*), palmitate-LPS treated TRIF deficient macrophages had a similar phenotype to palmitate alone treated cells (Fig. 6I, *black vs. green lines*).

Over-expression of the lysosomal biogenesis transcription factor TFEB attenuates cell death induced by palmitate and LPS

Our data suggested that inflammatory stress under lipotoxic conditions causes lysosome dysfunction and/or loss that contributes to macrophage cell death. Transcription factor EB (TFEB) controls a gene expression program that stimulates lysosomal biogenesis and degradative function and has been previously shown to improve cell viability in the setting of lysosomal dysfunction and/or depletion (45, 48–50). Thus, we tested whether gain-of-function of TFEB could reduce cell death and prevent lysosomal depletion following palmitate-LPS treatment. Since peritoneal macrophages are not readily transfectable, these experiments were performed in HEK293-TLR4/MD2/CD14 (HEK) cells, in which palmitate-LPS stimulation induces synergistic cell death (Fig. 4B). HEK cells were transiently transfected with a biscistronic vector (IRES) encoding GFP with and without TFEB sequences. Using flow cytometry to detect GFP expressing cells, we determined ~ 29% of the cells expressed GFP at 72 h (Fig 7A). TFEB expression at the protein level was also confirmed via western blotting in cells that had received the TFEB-containing plasmid (Fig. 7B). To determine the effect of TFEB over-expression on cell viability in response to palmitate-LPS, we gated on GFP^+ cells and determined viability by PI staining alone, since the GFP marker precluded concomitant FITC-annexin staining. Cells transfected with TFEB demonstrated significantly improved survival compared to cells with control (GFP only) vector (Fig 7C). In TFEB-transfected wells, untransfected cells (GFP^-) had a death phenotype similar to control-transfected cells. Thus, TFEB-mediated protection from cell death occurred in a cell autonomous fashion (Fig. 7D).

In a parallel set of samples we also assessed the lysosomal compartment in transfected cells using lysotracker red. GFP^+ cells from control vector samples demonstrated the expected decrease in lysotracker red staining following palmitate-LPS treatment (Fig 7E). In contrast, lysosomal fluorescence only minimally decreased in TFEB transfected cells stimulated with palmitate-LPS (Fig. 7F). Thus, TFEB overexpression protects cells from lysosomal depletion and cell death.

Discussion

Macrophages play a critical role in coordinating the host response to infection and tissue damage, both of which are impaired in diabetics. Thus, we investigated the impact of lipid excess, a common feature of these metabolic diseases (48), on macrophage responses to inflammatory stimuli. To assess the impact of saturated fatty acids on macrophage inflammatory function we stimulated peritoneal macrophages with LPS in the presence of palmitate. The combination of palmitate and TLR4 activation led to synergistic macrophage cell death through a pathway with features of both apoptosis (caspase-dependent) and necrosis (caspase-independent). Surprisingly, this synergistic death response was not dependent on ER stress, ceramide generation, or oxidative stress. While signaling via the TLR4 adaptor TRIF was required for macrophage death following palmitate-LPS challenge, this occurred independent of NF-κB, MAP kinases, and IRF3. Instead we found that the combination of palmitate and LPS led to lysosome depletion and/or destabilization. Cell death was markedly attenuated by over-expression of the lysosome-biogenesis factor TFEB, suggesting that restoring lysosome function could be an important strategy to reduce macrophage death under lipotoxic conditions.

TLR4 is a sensor for danger signals elaborated in response to both infectious organisms and sterile tissue damage (51–53). Therefore, dissecting the mechanisms by which lipids influence TLR4-mediated responses has the potential to be relevant to a broad spectrum of inflammatory states. We utilized ultrapure LPS, a prototypical TLR4 agonist, at concentrations sufficient to activate canonical downstream signaling pathways, but which, in

the absence of additional stimuli, does not cause cell death. To mimic the effects of dyslipidemia in cell culture, we supplemented culture media with palmitate, one of the most abundant of the dietary saturated fatty acids. In fibroblasts, myoblasts, endothelial cells, and β-cells, palmitate by itself at high concentrations is toxic and has therefore been used as a model stimulus for lipotoxicity. In these cell types, ER stress, de novo ceramide synthesis, and oxidative stress appear to play key roles in the cytotoxic effects of palmitate (21). The precise concentration of palmitate required to cause cell death is highly cell-type-dependent. In order to specifically address the effects of lipid overload on inflammatory signaling in macrophages, we chose concentrations of palmitate to model pathophysiological exposures (250 μM for pMACs and RAW cells, 750 μM for HEK cell system), but which led to only modest increases in cell death in the absence of additional stimuli.

In the present study we used thioglycollate elicited peritoneal cells as a model of mature macrophages. Less than 5% of the recovered elicited primary cells were SiglecF^{+}, F4/80^{+}, suggesting minimal contamination with eosinophils. These cells have the advantage of representing a more differentiated inflammatory cell, such as would be recruited to sites of injury, and are a well-established model for the assessment of macrophage inflammatory function (54). However, because thioglycollate elicitation could influence the biology of these cells, we also evaluated the effect of palmitate and LPS on RAW 264.7 cells and the human cell line HEK293 transfected with the macrophage LPS receptor complex. Similar to the peritoneal macrophages, both of these cell types also demonstrated synergistic cell death in the presence of palmitate and LPS.

Saturated fatty acids such as palmitate have been reported to activate TLR4 signaling at concentrations similar to those used in our experiments (22, 55). However, many BSA preparations have been shown to contain TLR2 and TLR4 ligands, which could complicate the interpretation of these studies (23). In our study, we solubilized palmitate by complexing it to ultrapure BSA, which alone did not increase TNFα mRNA or protein expression (our unpublished observations). While palmitate did not direct activate inflammatory pathways at the concentrations we used, it profoundly affected the phenotype of LPS activated macrophages and triggered a synergistic death response. This synergy required the TLR4 adaptor TRIF, but not the downstream transcription factor IRF3. These findings suggest that TRIF modulates cell death through a non-transcriptional mechanism. Of note, TRIF has a RIP homotypic interaction motif (RHIM) that can physically interact with death inducing molecules such as RIP1, RIP3, and caspase 8 (56). However, our data showing minimal protection from cell death with a pan-caspase inhibitor (ZVAD) and the RIP1 kinase inhibitor (nec 1) argues against an upstream role for a TRIF-RIP-caspase complex in this death mechanism (56, 57).

The death induced by LPS and palmitate has features of both apoptosis and necrosis by ANX-PI staining and subG1 DNA analysis. Caspase inhibition reduced apoptosis, but did not influence necrosis, suggesting that these death pathways can be dissociated. We considered that the inflammasome might also influence our death pathway as this response can occur with palmitate and LPS stimulation and may involve TRIF activation (58, 59). However, ZVAD is a potent caspase 1 and 11 inhibitor, and its failure to block palmitate-LPS synergistic cell death does not support a role for death by pyroptosis in our system.

Lysosomal damage and dysfunction can induce apoptotic-like and necrotic cell death responses (43). Our data showing early loss of the functional lysosomal compartment following palmitate-LPS stimulation and protection against synergistic death by cathepsin inhibition or TFEB overexpression support a model in which lysosomal dysfunction contributes to the synergistic cell death response. The partial nature of protection afforded by cathepsin B inhibition suggests that either additional molecules released from damaged

lysosomes contribute to the observed effects, or that the release of these enzymes is an amplification event that only occurs once membrane integrity is lost. Interestingly, lysosome dysfunction, depletion, and permeablization have been described in lysosomal storage diseases and neurodegenerative diseases (e.g., Parkinson's, Huntington's, and Alzheimer's disease), and forced expression of TFEB can reduce cell death in these systems as well (45, 49, 60, 61). Thus, it is conceivable that lysosome dysfunction leads to accumulation of cellular toxins, which ultimately promote loss of lysosomal membrane integrity and cell death. Given the diverse effects of TFEB on lysosomal biology, our results cannot distinguish whether rescue is a consequence of enhanced lysosomal degradative function, increased exocotyosis of cell toxins, or enhanced autophagy. Future experiments to probe the effects of membrane remodeling on lysosome function under lipotoxic conditions and to explore the mechanism(s) of TFEB rescue from palmitate-LPS stress will provide further insights into crosstalk between metabolic stress and inflammatory signaling.

In summary, we describe a novel macrophage cell death pathway that occurs when TLR4 is activated under lipotoxic conditions. The mechanism of this response involves the intersection between TRIF signaling and impaired lysosome function and integrity. We provide evidence that enhancing the lysosome compartment via TFEB over-expression can attenuate cell death in this circumstance, suggesting that modulation of lysosome function and/or targeted TFEB activation may be useful strategies for mitigating fatty acid-induced macrophage dysfunction in diabetic complications such as impaired host responses to infection and/or tissue injury.

Acknowledgments

We thank Marco Colonna, Michael Diamond and Michael Karin for generously providing KO mouse lines; Jin-Moo Lee for providing the pAAV bicistronic backbone for TFEB cloning; and Rohini Sidhu and Hideji Fujiwara for assistance with mass spectrometry, which was performed in the Washington University Metabolomics Facility.

References

1. Joshi N, Caputo GM, Weitekamp MR, Karchmer AW. Infections in patients with diabetes mellitus. N Engl J Med. 1999; 341:1906–1912. [PubMed: 10601511]
2. Rosen DA, Hung CS, Kline KA, Hultgren SJ. Streptozocin-induced diabetic mouse model of urinary tract infection. Infect Immun. 2008; 76:4290–4298. [PubMed: 18644886]
3. Czyzk A, Krolewski AS, Szablowska S, Alot A, Kopczynski J. Clinical course of myocardial infarction among diabetic patients. Diabetes Care. 1980; 3:526–529. [PubMed: 7460722]
4. Greer JJ, Ware DP, Lefer DJ. Myocardial infarction and heart failure in the db/db diabetic mouse. Am J Physiol Heart Circ Physiol. 2006; 290:H146–153. [PubMed: 16113078]
5. Lavaud S, Michel O, Sassy-Prigent C, Heudes D, Bazin R, Bariety J, Chevalier J. Early influx of glomerular macrophages precedes glomerulosclerosis in the obese Zucker rat model. J Am Soc Nephrol. 1996; 7:2604–2615. [PubMed: 8989739]
6. Sassy-Prigent C, Heudes D, Mandet C, Belair MF, Michel O, Perdereau B, Bariety J, Bruneval P. Early glomerular macrophage recruitment in streptozotocin-induced diabetic rats. Diabetes. 2000; 49:466–475. [PubMed: 10868970]
7. Wetzler C, Kampfer H, Stallmeyer B, Pfeilschifter J, Frank S. Large and sustained induction of chemokines during impaired wound healing in the genetically diabetic mouse: prolonged persistence of neutrophils and macrophages during the late phase of repair. J Invest Dermatol. 2000; 115:245–253. [PubMed: 10951242]
8. Ko HJ, Zhang Z, Jung DY, Jun JY, Ma Z, Jones KE, Chan SY, Kim JK. Nutrient stress activates inflammation and reduces glucose metabolism by suppressing AMP-activated protein kinase in the heart. Diabetes. 2009; 58:2536–2546. [PubMed: 19690060]

9. Oyama J, Blais C Jr, Liu X, Pu M, Kobzik L, Kelly RA, Bourcier T. Reduced myocardial ischemia-reperfusion injury in toll-like receptor 4-deficient mice. Circulation. 2004; 109:784–789. [PubMed: 14970116]
10. Kaisho T, Akira S. Critical roles of Toll-like receptors in host defense. Critical Reviews in Immunology. 2000; 20:393–405. [PubMed: 11145217]
11. Takeda K, Akira S. Toll receptors and pathogen resistance. Cellular Microbiology. 2003; 5:143–153. [PubMed: 12614458]
12. Li W, Sama AE, Wang H. Role of HMGB1 in cardiovascular diseases. Curr Opin Pharmacol. 2006; 6:130–135. [PubMed: 16487750]
13. Kaczorowski DJ, Tsung A, Billiar TR. Innate immune mechanisms in ischemia/reperfusion. Front Biosci (Elite Ed). 2009; 1:91–98. [PubMed: 19482628]
14. Takeuchi O, Hoshino K, Kawai T, Sanjo H, Takada H, Ogawa T, Takeda K, Akira S. Differential roles of TLR2 and TLR4 in recognition of gram-negative and gram-positive bacterial cell wall components. Immunity. 1999; 11:443–451. [PubMed: 10549626]
15. Takeda K, Akira S. TLR signaling pathways. Seminars in Immunology. 2004; 16:3–9. [PubMed: 14751757]
16. Brown J, Wang H, Hajishengallis GN, Martin M. TLR-signaling networks: an integration of adaptor molecules, kinases, and cross-talk. J Dent Res. 2011; 90:417–427. [PubMed: 20940366]
17. Oh DY, Morinaga H, Talukdar S, Bae EJ, Olefsky JM. Increased Macrophage Migration Into Adipose Tissue in Obese Mice. Diabetes. 2011
18. Chawla A, Nguyen KD, Goh YP. Macrophage-mediated inflammation in metabolic disease. Nature reviews Immunology. 2011; 11:738–749.
19. Assimacopoulos-Jeannet F. Fat storage in pancreas and in insulin-sensitive tissues in pathogenesis of type 2 diabetes. Int J Obes Relat Metab Disord. 2004; 28(Suppl 4):S53–57. [PubMed: 15592487]
20. Cascio G, Schiera G, Di Liegro I. Dietary fatty acids in metabolic syndrome, diabetes and cardiovascular diseases. Curr Diabetes Rev. 2012; 8:2–17. [PubMed: 22414056]
21. Brookheart RT, Michel CI, Schaffer JE. As a matter of fat. Cell Metab. 2009; 10:9–12. [PubMed: 19583949]
22. Shi H, Kokoeva MV, Inouye K, Tzameli I, Yin H, Flier JS. TLR4 links innate immunity and fatty acid-induced insulin resistance. J Clin Invest. 2006; 116:3015–3025. [PubMed: 17053832]
23. Erridge C, Samani NJ. Saturated fatty acids do not directly stimulate Toll-like receptor signaling. Arterioscler Thromb Vasc Biol. 2009; 29:1944–1949. [PubMed: 19661481]
24. Misharin AV, Saber R, Perlman H. Eosinophil contamination of thioglycollate-elicited peritoneal macrophage cultures skews the functional readouts of in vitro assays. J Leukoc Biol. 2012; 92:325–331. [PubMed: 22706315]
25. Listenberger LL, Ory DS, Schaffer JE. Palmitate-induced apoptosis can occur through a ceramide-independent pathway. J Biol Chem. 2001; 276:14890–14895. [PubMed: 11278654]
26. Juan, Da. Current Protocols in Cytometry. Robinson, JP., editor. J. Wiley and Sons; 1997. p. 7.5.1-7.5.24.
27. Listenberger LL, Han X, Lewis SE, Cases S, Farese RV Jr, Ory DS, Schaffer JE. Triglyceride accumulation protects against fatty acid-induced lipotoxicity. Proc Natl Acad Sci U S A. 2003; 100:3077–3082. [PubMed: 12629214]
28. Djouadi F, Bonnefont JP, Munnich A, Bastin J. Characterization of fatty acid oxidation in human muscle mitochondria and myoblasts. Molecular Genetics and Metabolism. 2003; 78:112–118. [PubMed: 12618083]
29. Schnute ME, McReynolds MD, Kasten T, Yates M, Jerome G, Rains JW, Hall T, Chrencik J, Kraus M, Cronin CN, Saabye M, Highkin MK, Broadus R, Ogawa S, Cukyne K, Zawadzke LE, Peterkin V, Iyanar K, Scholten JA, Wendling J, Fujiwara H, Nemirovskiy O, Wittwer AJ, Nagiec MM. Modulation of cellular S1P levels with a novel, potent and specific inhibitor of sphingosine kinase-1. Biochem J. 2012; 444:79–88. [PubMed: 22397330]
30. Spector AA. Fatty acid binding to plasma albumin. J Lipid Res. 1975; 16:165–179. [PubMed: 236351]

31. Kleinfeld AM, Prothro D, Brown DL, Davis RC, Richieri GV, DeMaria A. Increases in serum unbound free fatty acid levels following coronary angioplasty. Am J Cardiol. 1996; 78:1350–1354. [PubMed: 8970405]
32. El-Assaad W, Buteau J, Peyot ML, Nolan C, Roduit R, Hardy S, Joly E, Dbaibo G, Rosenberg L, Prentki M. Saturated fatty acids synergize with elevated glucose to cause pancreatic beta-cell death. Endocrinology. 2003; 144:4154–4163. [PubMed: 12933690]
33. Laybutt DR, Preston AM, Akerfeldt MC, Kench JG, Busch AK, Biankin AV, Biden TJ. Endoplasmic reticulum stress contributes to beta cell apoptosis in type 2 diabetes. Diabetologia. 2007; 50:752–763. [PubMed: 17268797]
34. Wei Y, Wang D, Topczewski F, Pagliassotti MJ. Saturated fatty acids induce endoplasmic reticulum stress and apoptosis independently of ceramide in liver cells. Am J Physiol Endocrinol Metab. 2006; 291:E275–281. [PubMed: 16492686]
35. Listenberger LL, Schaffer JE. Mechanisms of lipoapoptosis: implications for human heart disease. Trends Cardiovasc Med. 2002; 12:134–138. [PubMed: 12007739]
36. Pfaffenbach KT, Gentile CL, Nivala AM, Wang D, Wei Y, Pagliassotti MJ. Linking endoplasmic reticulum stress to cell death in hepatocytes: roles of C/EBP homologous protein and chemical chaperones in palmitate-mediated cell death. Am J Physiol Endocrinol Metab. 2010; 298:E1027–1035. [PubMed: 20159858]
37. Yamamoto M, Sato S, Mori K, Hoshino K, Takeuchi O, Takeda K, Akira S. Cutting edge: a novel Toll/IL-1 receptor domain-containing adapter that preferentially activates the IFN-beta promoter in the Toll-like receptor signaling. J Immunol. 2002; 169:6668–6672. [PubMed: 12471095]
38. Wang Q, McLoughlin RM, Cobb BA, Charrel-Dennis M, Zaleski KJ, Golenbock D, Tzianabos AO, Kasper DL. A bacterial carbohydrate links innate and adaptive responses through Toll-like receptor 2. J Exp Med. 2006; 203:2853–2863. [PubMed: 17178920]
39. Medzhitov R, Preston-Hurlburt P, Kopp E, Stadlen A, Chen C, Ghosh S, Janeway CA Jr. MyD88 is an adaptor protein in the hToll/IL-1 receptor family signaling pathways. Molecular Cell. 1998; 2:253–258. [PubMed: 9734363]
40. Chow JC, Young DW, Golenbock DT, Christ WJ, Gusovsky F. Toll-like receptor-4 mediates lipopolysaccharide-induced signal transduction. J Biol Chem. 1999; 274:10689–10692. [PubMed: 10196138]
41. Ostrander DB, Sparagna GC, Amoscato AA, McMillin JB, Dowhan W. Decreased cardiolipin synthesis corresponds with cytochrome c release in palmitate-induced cardiomyocyte apoptosis. J Biol Chem. 2001; 276:38061–38067. [PubMed: 11500520]
42. Borradaile NM, Han X, Harp JD, Gale SE, Ory DS, Schaffer JE. Disruption of endoplasmic reticulum structure and integrity in lipotoxic cell death. J Lipid Res. 2006; 47:2726–2737. [PubMed: 16960261]
43. Hafner Cesen M, Pegan K, Spes A, Turk B. Lysosomal pathways to cell death and their therapeutic applications. Experimental Cell Research. 2012; 318:1245–1251. [PubMed: 22465226]
44. Repnik U, Stoka V, Turk V, Turk B. Lysosomes and lysosomal cathepsins in cell death. Biochim Biophys Acta. 2012; 1824:22–33. [PubMed: 21914490]
45. Dehay B, Bove J, Rodriguez-Muela N, Perier C, Recasens A, Boya P, Vila M. Pathogenic lysosomal depletion in Parkinson's disease. J Neurosci. 2010; 30:12535–12544. [PubMed: 20844148]
46. Nylandsted J, Gyrd-Hansen M, Danielewicz A, Fehrenbacher N, Lademann U, Hoyer-Hansen M, Weber E, Multhoff G, Rohde M, Jaattela M. Heat shock protein 70 promotes cell survival by inhibiting lysosomal membrane permeabilization. J Exp Med. 2004; 200:425–435. [PubMed: 15314073]
47. Stoka V, Turk B, Schendel SL, Kim TH, Cirman T, Snipas SJ, Ellerby LM, Bredesen D, Freeze H, Abrahamson M, Bromme D, Krajewski S, Reed JC, Yin XM, Turk V, Salvesen GS. Lysosomal protease pathways to apoptosis. Cleavage of bid, not pro-caspases, is the most likely route. J Biol Chem. 2001; 276:3149–3157. [PubMed: 11073962]
48. Pena-Llopis S, Brugarolas J. TFEB, a novel mTORC1 effector implicated in lysosome biogenesis, endocytosis and autophagy. Cell Cycle. 2011; 10:3987–3988. [PubMed: 22101272]

49. Medina DL, Fraldi A, Bouche V, Annunziata F, Mansueto G, Spampanato C, Puri C, Pignata A, Martina JA, Sardiello M, Palmieri M, Polishchuk R, Puertollano R, Ballabio A. Transcriptional activation of lysosomal exocytosis promotes cellular clearance. Developmental Cell. 2011; 21:421–430. [PubMed: 21889421]
50. Ma X, Godar RJ, Liu H, Diwan A. Enhancing lysosome biogenesis attenuates BNIP3-induced cardiomyocyte death. Autophagy. 2012; 8
51. Andersson U, Tracey KJ. HMGB1 is a therapeutic target for sterile inflammation and infection. Annual Review of Immunology. 2011; 29:139–162.
52. Bjorkbacka H. Multiple roles of Toll-like receptor signaling in atherosclerosis. Curr Opin Lipidol. 2006; 17:527–533. [PubMed: 16960501]
53. Chao W. Toll-like receptor signaling: a critical modulator of cell survival and ischemic injury in the heart. Am J Physiol Heart Circ Physiol. 2009; 296:H1–12. [PubMed: 19011041]
54. Saitoh T, Fujita N, Jang MH, Uematsu S, Yang BG, Satoh T, Omori H, Noda T, Yamamoto N, Komatsu M, Tanaka K, Kawai T, Tsujimura T, Takeuchi O, Yoshimori T, Akira S. Loss of the autophagy protein Atg16L1 enhances endotoxin-induced IL-1beta production. Nature. 2008; 456:264–268. [PubMed: 18849965]
55. Weatherill AR, Lee JY, Zhao L, Lemay DG, Youn HS, Hwang DH. Saturated and poly unsaturated fatty acids reciprocally modulate dendritic cell functions mediated through TLR4. J Immunol. 2005; 174:5390–5397. [PubMed: 15843537]
56. Kaiser WJ, Offermann MK. Apoptosis induced by the toll-like receptor adaptor TRIF is dependent on its receptor interacting protein homotypic interaction motif. J Immunol. 2005; 174:4942–4952. [PubMed: 15814722]
57. Feoktistova M, Geserick P, Kellert B, Dimitrova DP, Langlais C, Hupe M, Cain K, MacFarlane M, Hacker G, Leverkus M. cIAPs block Ripoptosome formation, a RIP1/caspase-8 containing intracellular cell death complex differentially regulated by cFLIP isoforms. Molecular Cell. 2011; 43:449–463. [PubMed: 21737330]
58. Wen H, Gris D, Lei Y, Jha S, Zhang L, Huang MT, Brickey WJ, Ting JP. Fatty acid-induced NLRP3-ASC inflammasome activation interferes with insulin signaling. Nature Immunology. 2011; 12:408–415. [PubMed: 21478880]
59. Rathinam VA, Vanaja SK, Waggoner L, Sokolovska A, Becker C, Stuart LM, Leong JM, Fitzgerald KA. TRIF Licenses Caspase-11-Dependent NLRP3 Inflammasome Activation by Gram-Negative Bacteria. Cell. 2012
60. Ditaranto K, Tekirian TL, Yang AJ. Lysosomal membrane damage in soluble Abeta-mediated cell death in Alzheimer's disease. Neurobiology of Disease. 2001; 8:19–31. [PubMed: 11162237]
61. Tsunemi T, Ashe TD, Morrison BE, Soriano KR, Au J, Roque RA, Lazarowski ER, Damian VA, Masliah E, La Spada AR. PGC-1alpha Rescues Huntington's Disease Proteotoxicity by Preventing Oxidative Stress and Promoting TFEB Function. Science Translational Medicine. 2012; 4:142ra197.

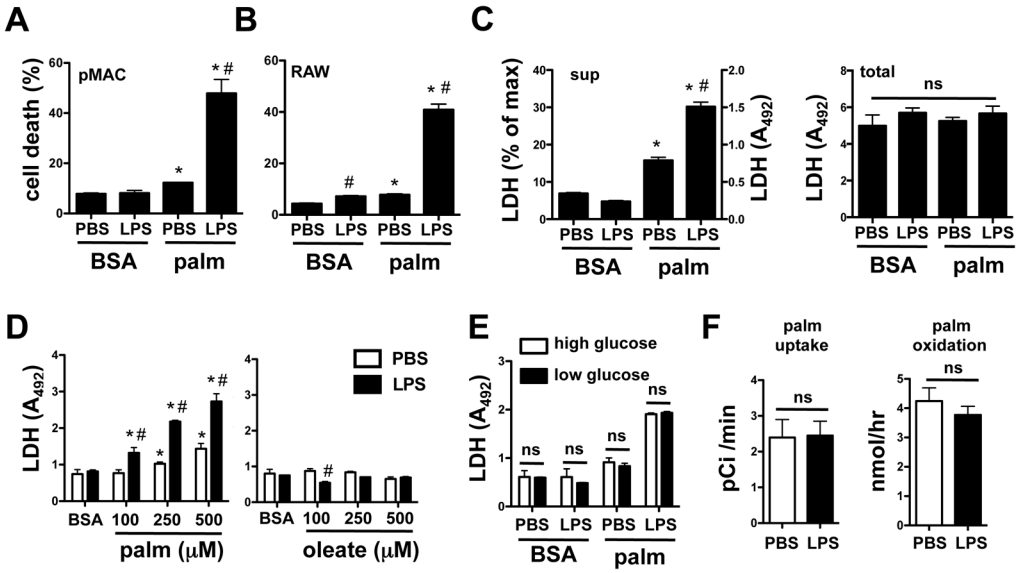

Figure 1. Palmitate and LPS lead to synergistic cell death in macrophages

(**A, B**) Peritoneal macrophages (pMACs, **A**) or RAW 264.7 cells **(B)** were stimulated with PBS or 50 ng/ml LPS in the presence of 250 μM palmitate (palm) complexed to BSA or in the presence of BSA alone. Cell death was assessed by annexin (ANX)-propidium iodide (PI) flow cytometry at 24 h on 10^4 cells/sample. Graphs report cell death as percent of the total cells that were either ANX^+/PI^- or ANX^+/PI^+. (**C**) Following stimulation of pMACS as indicated, LDH was quantified in the supernatant (sup) and is reported as absorbance at 492 nm and as percent of total cellular LDH (*left panel*). Total cellular LDH following lysis is shown for each of the treatments (*right panel*). (**D**) pMACs were stimulated with increasing concentrations of palm (*left panel*) or oleate (*right panel*) in the presence of PBS or LPS and cell death was assessed by LDH release. (**E**) pMACs were stimulated with palm and LPS in either high (4.5 g/L, *white bars*) or low (1 g/L, *black bars*) glucose media and cell death was determined by LDH release. (**F**) Rates of ^{14}C-palm uptake (*left panel*) and oxidation (*right panel*) were determined following LPS stimulation. All experiments were performed a minimum of 3 times in triplicate. Bars represent the mean ± SE. *, $p \leq 0.05$ for BSA vs. palm; #, $p \leq 0.05$ for PBS vs. LPS; ns, non-significant.

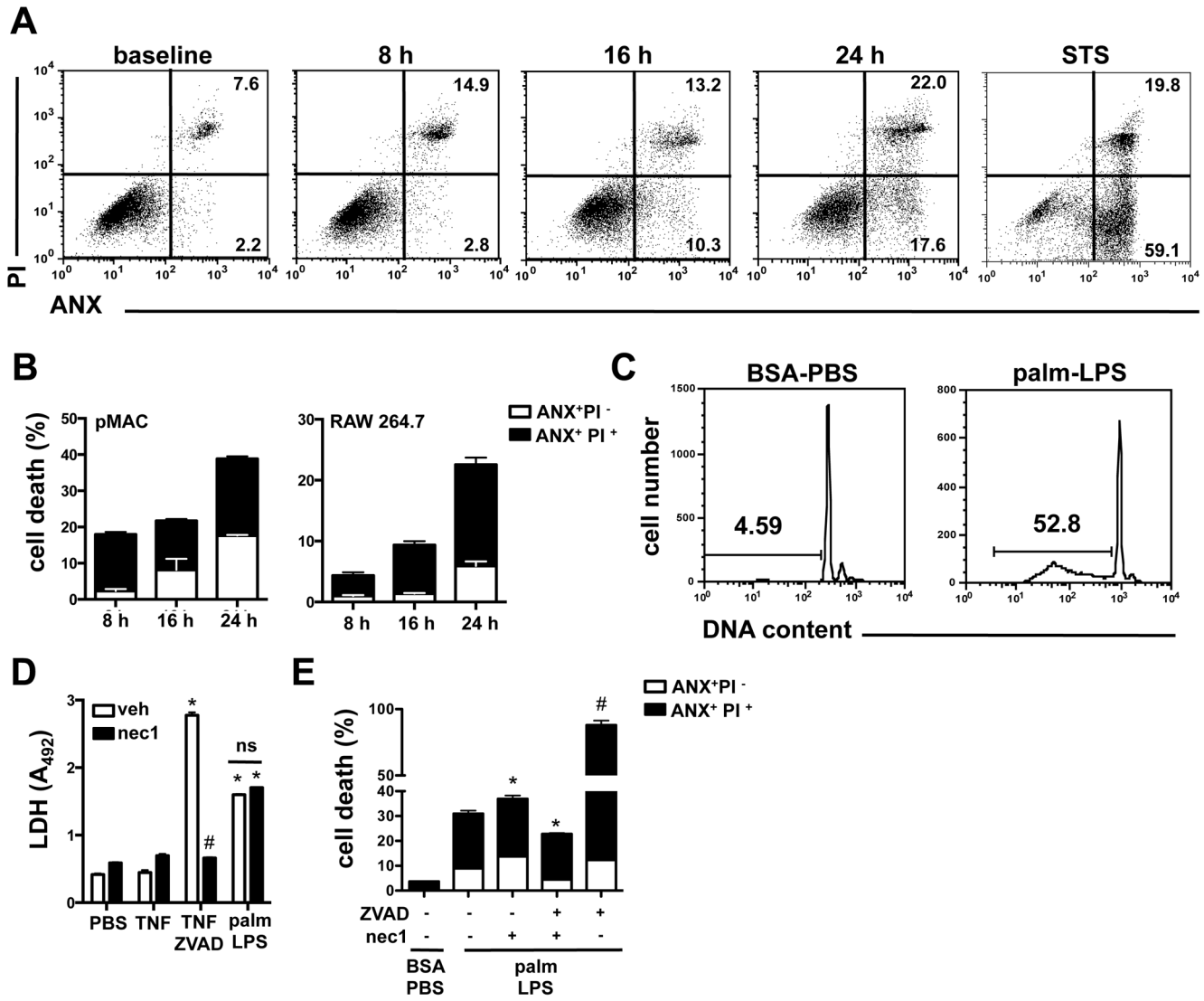

Figure 2. LPS and palmitate-mediated synergistic cell death has features of apoptosis and necrosis

(**A**) pMACs were stimulated with 50 ng/ml of LPS and 250 μM palm or 80 nM staurosporine (STS) and cell death was assessed by ANX-PI flow cytometry at the indicated timepoints. Representative flow plots are shown with percent apoptotic (ANX^+PI^-) and necrotic cells (ANX^+PI^+) indicated in the lower and upper right quadrants, respectively. (**B**) pMACs (*left panel*) or RAW 264.7 cells (*right panel*) were stimulated with palm-LPS for the indicated times and the proportions of ANX^+PI^- (white bar) and ANX^+PI^+ (black bars) cells are shown **(C)** pMACs were stimulated with BSA-PBS or palm-LPS for 16 h, and sub-G1 DNA was assessed by PI staining of permeablized cells. Representative histograms are shown with the percent of cells containing cleaved DNA indicated by the gate. (**D**) Macrophages were treated as indicated in the presence of vehicle (*white bars*) or necrostatin 1 (nec1, *black bars*, 50 μM) and LDH release was quantified (**E**) pMACs were stimulated with palm-LPS in the presence of vehicle, ZVAD (20 μM), and/or nec1 (50 μM) for 24 h and cell death was determined by ANX-PI staining. The white and black colored portion of the bars represent the percent of cells that were ANX^+/PI^- and ANX^+/PI^+, respectively. Bars

represent mean ± SE. *, $p \leq 0.05$ for BSA-PBS vs. palm-LPS; #, $p \leq 0.05$ for veh vs. inhibitor; ns, non significant.

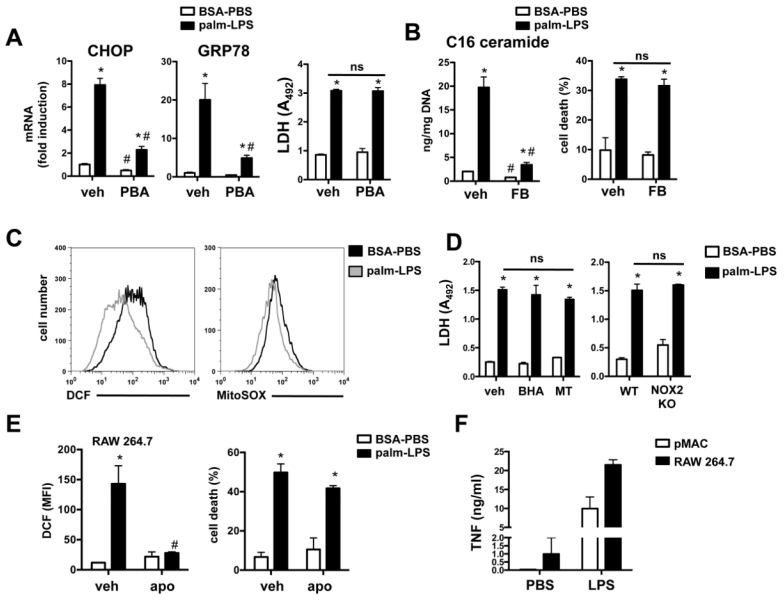

Figure 3. The cell death pathway activated by palmitate and LPS is largely independent of ER stress, ceramide, and ROS pathways

(**A**) pMACs were stimulated with palm ± LPS in the presence of phenylbutyric acid (PBA) or vehicle (veh). Expression of ER stress markers was quantified by qRT-PCR (at 16 h) and cell death was determined by LDH release (at 20h). (**B**) C16 ceramide was quantified by LC-MS/MS in pMACs pre-treated with veh or 5 μM fumonisin B (FB) 16 h after stimulation. Cell death was determined by ANX-PI flow cytometry. (**C**) pMACs were stimulated as indicated for 16 h, and oxidative stress was determined by DCF (*left panel*) or MitoSOX (*right panel*) staining and flow cytometry analysis. Representative histograms are shown. (**D**) WT macrophages were treated with palm-LPS in the presence of the antioxidants butylated hydroxyanisole (BHT, 100 μM) or mito-TEMPO (MT, 500 μM) (*left panel*) or compared to NOX2 KO mice (*right panel*) and cell death was determined at 20 h by LDH release. (**E**) RAW 264.7 cells were stimulated with palm-LPS in the presence of veh or apocynin (apo) and ROS/DCF (*left panel*) or cell death (*right panel*) was determined by flow cytometry. (**F**) pMACs (white bars) or RAW 264.7 cells (black bars) were stimulated with PBS or LPS and TNFα secretion was quantified at 16 h. All experiments were performed a minimum of 3 times in triplicate. Bars represent mean ± SE. *, $p \leq 0.05$ for BSA-PBS vs. palm-LPS; #, $p \leq 0.05$ for veh vs. inhibitor or WT vs. KO; ns, non significant.

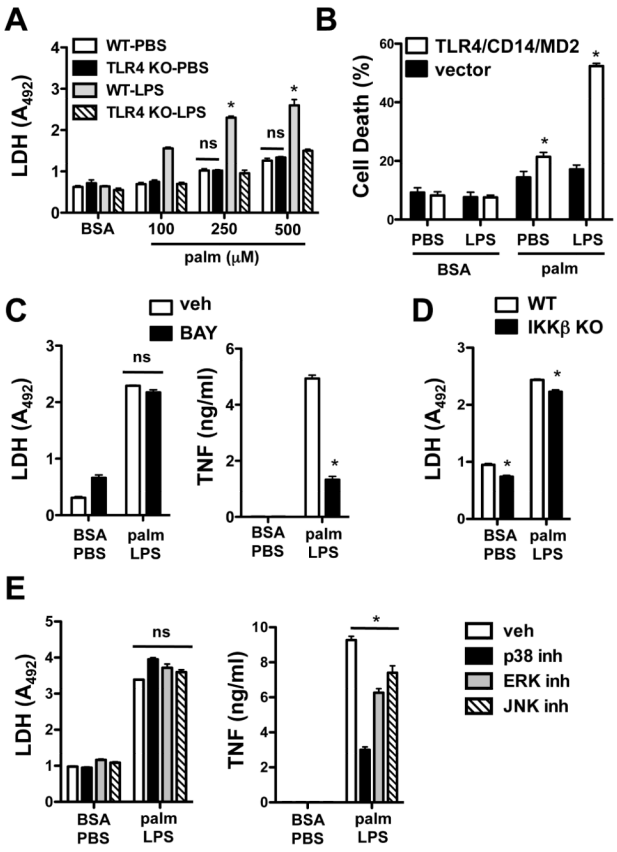

Figure 4. Synergistic cell death is TLR4-dependent, but independent of NF-κB and MAP kinase activation

(**A**) pMACs from WT or TLR4 KO mice were stimulated with the indicated concentrations of palm ± LPS and cell death was determined by LDH release at 20 h. (**B**) HEK293 cells stably transfected with TLR4/CD14/MD2 or control vector were stimulated with 50 ng LPS in the presence of 750 μM palm or BSA. Cell death was determined by ANX-PI staining at 48 h. (**C**) WT macrophages were pre-treated with the NF-κB inhibitor BAY 11-7085 (BAY, 3.125 μM) followed by stimulation with BSA-PBS or 250 μM palm-LPS. Cell death was determined by LDH release at 20 h, and secretion of TNFα was quantified by ELISA. (**D**) IKKβ macrophage-specific KO cells were stimulated as indicated and cell death was assessed by LDH release at 20 h. (**E**) pMACs were pre-incubated with MAP kinase inhibitors (20 μM SB203580 for p38; 10 μM PD98059 for ERK; 20 μM SP600125 for JNK) followed by palm-LPS treatment. Cell death and TNFα secretion were determined at 20 h by LDH release and ELISA, respectively. All experiments were performed a minimum of 3 times in triplicate. Bars represent mean ± SE. *, $p \leq 0.05$ for vehicle vs. inhibitor or for WT vs. KO; ns, non-significant.

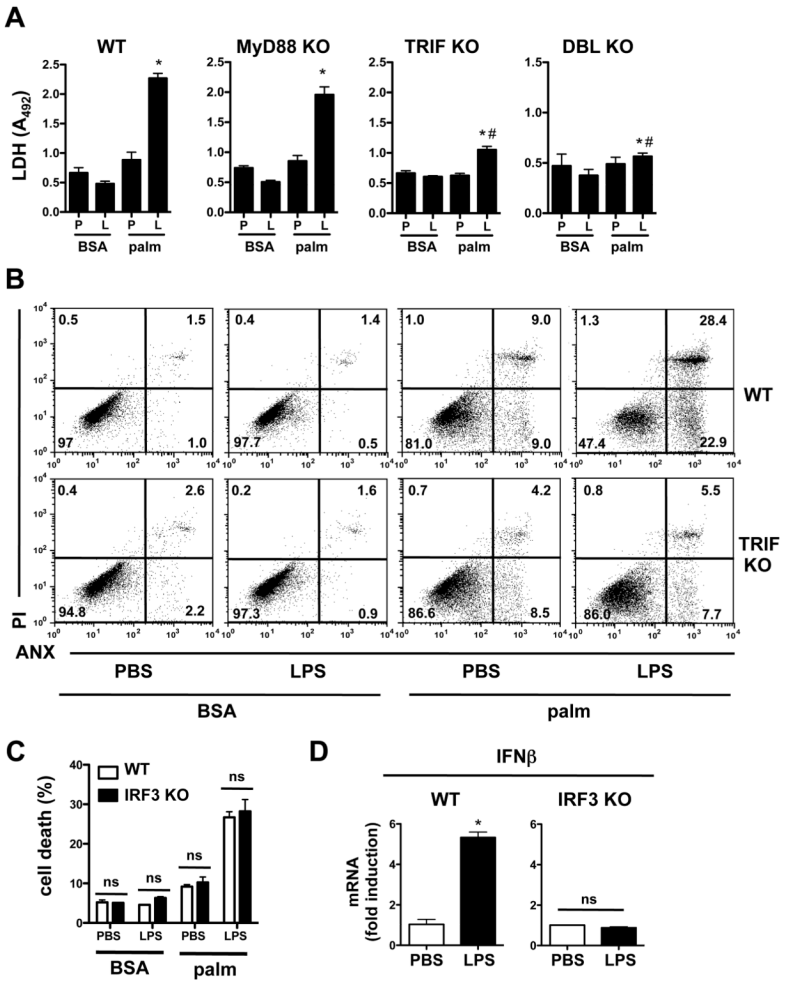

Figure 5. The induction of synergistic cell death by palmitate and TLR4 occurs via a TRIF-dependent, IRF3-independent mechanism

(**A**) Macrophages were isolated from WT mice or mice deficient in MyD88, TRIF, or both (DBL KO). Cell death was assessed by LDH release 20 h after the indicated stimulations (P, PBS; L, LPS). (**B**) WT or TRIF KO cells were stimulated as indicated and cell death was assessed by ANX–PI staining at 24 h. Representative flow cytometry plots are shown. (**C**) pMACs from WT or IRF3 KO mice were challenged with 250 μM palm +/− LPS and cell death was assessed by ANX-PI staining at 24 h. (**D**) mRNA was isolated from WT (*left panel*) or IRF3 KO (*right panel*) macrophages 1 h after LPS stimulation. IFNβ expression levels were determined by qRT-PCR. All experiments were performed a minimum of 3 times in triplicate. Bars represent mean ± SE. *, $p \leq 0.05$ for PBS vs. LPS; #, $p \leq 0.05$ for WT vs. KO; ns, non-significant.

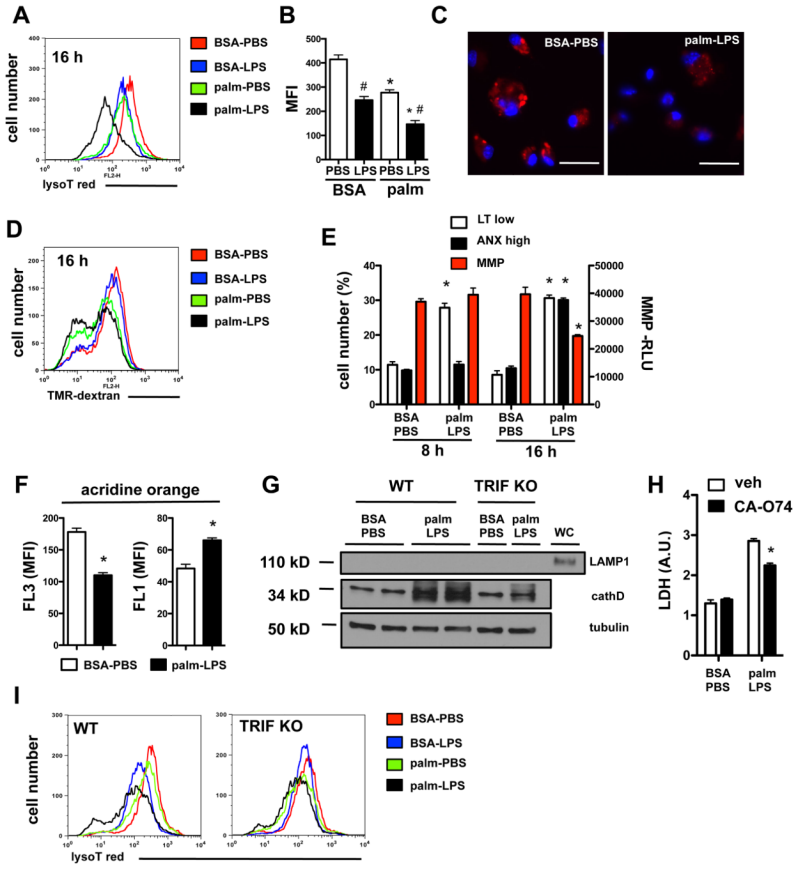

Figure 6. Early and sustained loss of lysosomes occurs in macrophages treated with palmitate and LPS

(**A–C**) pMACs were stimulated as indicated for 16 h and stained with lysotracker red (lysoT red) followed by by flow cytometry (**A, B**) or immunofluorescence (**C**). A representative plot (red, BSA-PBS; blue, BSA-LPS; green, palm-PBS; black, palm-LPS) (**A**), MFI quantification (**B**), and immunofluorescent image (**C**, bar 25 μm, lysotracker red, Hoechst nuclear dye blue) are shown. (**D**) pMACs were preloaded with tetramethylrhodamine(TMR)-dextran for 2 h and then treated with the indicated stimuli for 16 h followed by flow cytometry analysis. A representative histogram is shown. (**E**) Quantification of lysoT red low cells (LT low), annexin positive cells (ANX high), and mitochondrial membrane potential (MMP) at 8 h and 16 h after stimulation with BSA-PBS or palm-LPS. (**F**) pMACs were treated with BSA-PBS or palm-LPS for 16h followed by staining with acridine orange. Orange (FL3) and green (FL1) mean fluorescence intensity (MFI) was quantified by flow cytometry. (**G**) Cytoplasmic protein was isolated 16h after stimulation with BSA-PBS or palm-LPS in WT or TRIF KO cells and cathepsin D (cathD) levels were assessed by western blot. LAMP1 blotting was also performed to adequacy of fractionation. (**H**) pMACs were pre-treated with the cathepsin B inhibitor CAO-74 (10 μM) followed by BSA-PBS or palm-LPS and cell death was determined by LDH release at 20 h. (**I**) WT or TRIF KO pMACs were treated with BSA-PBS (red), BSA-LPS (blue), palm-PBS (green) or palm-LPS (black) for 16 h followed by lysoT red staining. Representative flow cytometry plots are shown. All experiments were performed a minimum of 3 times in triplicate. Graphs display mean ± SE. *, $p \leq 0.05$ for BSA vs. palm; #, $p \leq 0.05$ for PBS vs. LPS; ns, non-significant.

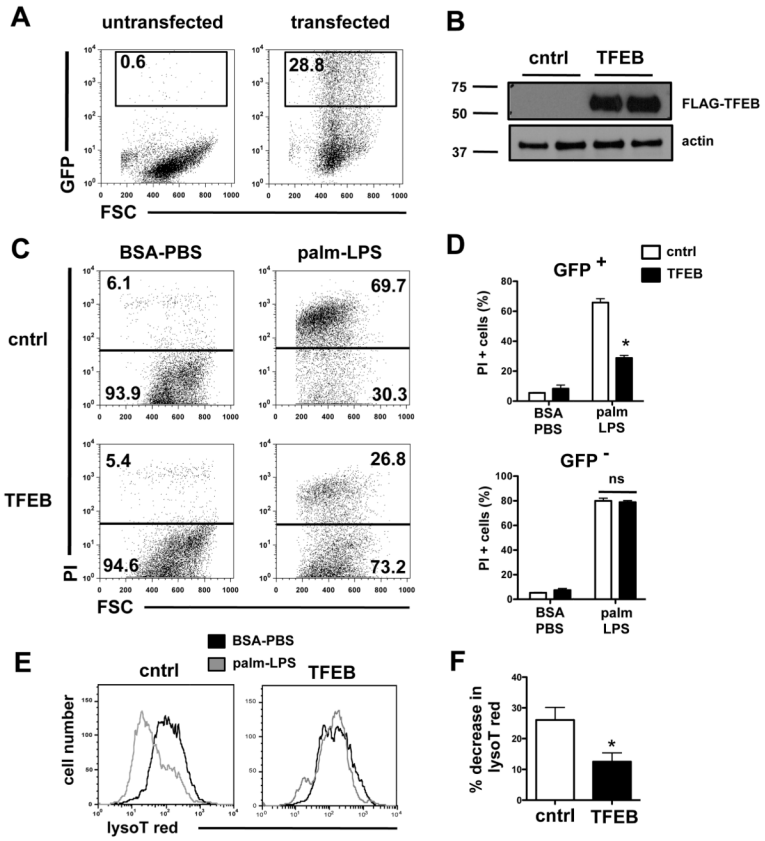

Figure 7. Over-expression of TFEB prevents lysosomal phenotype and rescues cell death induced by palmitate and LPS

HEK293-TLR4/CD14/MD2 cells were transfected control GFP vector (cntrl) or a FLAG-TFEB expression construct containing an IRES-GFP element. Cells were stimulated as indicated 24 h after transfection and flow cytomery was performed 48 h later. (**A**) Approximately 29% of the total cells expressed the GFP construct. (**B**) TFEB protein expression was assessed by western blot 24 h after transfection using α-FLAG antibody. Actin is shown as loading control. (**C, D**) 24 h following transfection, cells were stimulated with BSA-PBS or palm-LPS for 48 h, stained with PI and analyzed by flow cytometry. Representative dot plots from the GFP^+ cells are shown (**C**), and summed data for GFP^+ (*top panel*) and GFP^- (*bottom panel*) cells are plotted (**D**). (**E**) LysoT red fluorescence was assessed 48 h after stimulation with BSA-PBS (black) or palm-LPS (gray) in control vector and TFEB-transfected cells. Representative histograms are shown. (**F**) Quantification of the palm-LPS induced decrease in lysoT red fluorescence (MFI) in control and TFEB transfected cells. All experiments were performed a minimum of 3 times in triplicate. Bars represent mean ± SE. *, $p \leq 0.05$ for control vector vs. TFEB vector; ns, non-significant.